Quantitative void fraction measurement method by neutron radiography and applications to two-phase flow researches

Takenaka, Nobuyuki

Asano, Hitoshi

(Citation)
Experimental Thermal and Fluid Science,29(3):393-402

(Issue Date)
2005-03

(Resource Type)
journal article

(Version)
Accepted Manuscript

(URL)
https://hdl.handle.net/20.500.14094/90000204

QUANTITATIVE VOID FRACTION MEASUREMENT METHOD BY NEUTRON RADIOGRAPHY AND APPLICATIONS TO TWO-PHASE FLOW RESEARCHES

N. Takenaka* and H. Asano

Department of Mechanical Engineering, Kobe University
1-1 Rokkodai, Nada, Kobe 657-8501 Japan

* corresponding author, takenaka@mech.kobe-u.ac.jp

ABSTRACT

Quantitative void fraction measurement method by neutron radiography was developed using a neutron absorber grid based on an umbra method. The cross-sectionally averaged void fraction for various flow patterns in air-water two-phase flow in a tube was measured quantitatively. Uncertainty analyses were carried out for the measured values and the accuracy of the measurement was discussed for each flow pattern. Experimental results agree well with the prediction by drift flux model. The quantitative measurement method was applied to two-phase flow in a concentric annular tube, a tube with a spiral wire, a rod bundle, a capillary tube and a plate fin heat exchanger. The CT reconstruction method was applied to measure the quantitative void fraction distributions in the cross section.

1. INTRODUCTION

Visualization by neutron radiography is suitable for two-phase flow studies. Measurement of the void fraction is important to analyze the two-phase flow phenomena. However, it is not easy to measure the void fraction quantitatively from the images obtained by neutron radiography. The brightness of the image is not always proportional to the value calculated by linear attenuation equations.

Some methods have already been proposed for the quantitative measurement by neutron radiography. Glickstein et al. [1] used Monte-Carlo simulation for quantitative measurement and applied it to void fraction measurement by estimating the neutron scattering as an inverse problem of neutron interaction. No special experimental preparation is required with this method. The profile of the void fraction distribution should be assumed to obtain a unique answer to solve the inverse problem. Hirdlika and Peterka [2], Hibiki et al. [3] and Yoshii and Kobayashi [4] proposed to increase the distance between the converter and the object to reduce the possibility of the scattered neutrons falling on the image in the converter. This method is easy but the spatial resolution is reduced if the L/D of the system is not high.

Tamaki [5] inserted a collimator made of neutron absorber between the converter and the object to reduce the neutrons the direction of which was changed after scattering in the object. A honeycomb painted with Gadolium was tested. By changing the L/D of the honeycomb the reduction rate of the scattered neutrons could be estimated. When the L/D of the system was low, the visible field was quite reduced due to the shadow of the collimator on the converter. Kobayashi et al. [6] employed an umbra method to compensate the neutron scattering effects. A cadmium neutron absorber tape was placed between the object and the source to make the umbra of the tape on the converter. The brightness due to the scattered neutron could be measured by the brightness at the umbra. Compensation was made by subtracting the image with the tape from that without it. This method is expected to compensate the effects of the scattered scintillation optical rays. One-dimensional quantitative distribution along the tape is obtainable with this method. Murata et al. [7] modified this method to two-dimensional measurement by using a grid made of several tapes. The interval of the tapes should be long enough for avoiding the effects of other tapes. Several images with changing the position of the grid were required for two-dimensional measurement with reasonable spatial resolution.

Every method has merits and demerits so the best one should be chosen for the purpose of the measurement. However, the effects of the scattered optical rays can be compensated only by the umbra method. The scattering is caused by the reflection of the optical rays in the camera obscure. The effects should be considered when the neutron image is converted to optical rays, i.e., the TV system. There is no problem for film and imaging plate methods. The umbra method using a grid made of neutron absorber suitable for the void fraction measurement was developed [8].

The present authors have reported on visualization of various two-phase flow and three-dimensional void fraction distribution in a rod bundle by using a cooled CCD camera by thermal and fast neutron radiography [9]. The purpose of this report is to propose a method to measure the quantitative void fraction distribution in two-phase flows to discuss the accuracy and uncertainty analyses and to show quantitative measurement results for various two-phase flows.

2. QUANTITATIVE MEASUREMENT

Three images of the two-phase flow experimental test section are obtainable when it is filled with gas, liquid and two-phase mixture in the same configuration. The brightness of the images, $S(x,y)$, is expressed as below, where $G(x,y)$ and $O(x,y)$ are the gain and the offset, ρ and μ_m are the density and the mass attenuation coefficient of the object, α (x,y) and $t(x,y)$ are the void fraction averaged in the beam direction and the thickness of the flow channel, and the suffixes 1, 0, TP, w and L mean filled with the gas, with the liquid, with the two-phase mixture, the wall and the liquid, respectively.

filled with gas : $\alpha(x,y) = 1$

$$S_1(x,y) = G(x,y)\exp\left[-\rho_w \mu_{mw} t_w(x,y)\right] + O_1(x,y) \qquad (1)$$

filled with liquid : $\alpha(x,y) = 0$

$$S_1(x,y) = G(x,y)\exp\left[-\rho_w \mu_{mw} t_w(x,y) + \rho_L \mu_{mL} t(x,y)\right] + O_1(x,y) \qquad (2)$$

filled with two-phase mixture

$$S_{TP}(x,y) = G(x,y)\exp\left[-\rho_w \mu_{mw} t_w(x,y) + \{1-\alpha(x,y)\}\rho_L \mu_{mL} t(x,y)\right] + O_{TP}(x,y) \qquad (3)$$

$G(x,y)$, ρ_w, ρ_L, μ_{mw}, μ_{mL}, $t_w(x,y)$ and $t(x,y)$ are assumed to be constant. If the three values of $O(x,y)$ in the above equations are obtainable, $\alpha(x,y)$ can be determined without the constant values mentioned above as

$$\alpha(x,y) = \ln\left[\frac{S_{TP}(x,y) - O_{TP}(x,y)}{S_0(x,y) - O_0(x,y)}\right] \Big/ \ln\left[\frac{S_1(x,y) - O_1(x,y)}{S_0(x,y) - O_0(x,y)}\right] \qquad (4)$$

where the three terms of $\{S(x,y) - O(x,y)\}$ for the suffixes 0, 1, P indicate the attenuation terms in Eqs. (1)-(3)

Two kinds of the offsets should be considered. The offsets of the imaging system and the radioactive and the optical rays originated from the system besides the object are determined by its point (x, y) and are assumed to be the same in three images. However, the neutrons scattered in the object and the optical rays scattered in the camera system depend on the object. The offsets due to these effects are different in three images. The offset at the point (x, y) is affected by the other points (x', y') over the image and should be expressed as

$$O(x,y) = \iint O(x,y,x',y')dx'dy' \qquad (5)$$

The latter offset term expressed as Eq.(5) can not be determined by using the other images. Therefore, it is necessary to develop the processing method to obtain the offset $O(x,y)$ as well as the brightness $S(x,y)$ in one image for the quantitative measurement.

The umbra method was modified to measure both S(x,y) and $O(x,y)$ in one image in sacrifice of the

spatial image information. A grid made of B_4C, boron has high attenuation coefficient for thermal neutron, was placed between the object and the source. The image with the grid was not compared with the image without it in the previous methods [6], [7] but both values of *S(x,y)* and *O(x,y)* were determined by spatial interpolation in the image with the grid.

The compensated attenuation term, $\{S(x,y)-O(x,y)\}_c$, is estimated by the image calculation as

$$\{S(x,y)-O(x,y)\}_c = S(x,y)-\frac{S(x,y+\delta)+S(x,y-\delta)}{2} \qquad (6)$$

where δ is the width and the interval of the bars of the grid. Compensated values can be calculated with the brightness at the positions of (x,y) , $(x,y+\delta)$ and $(x,y-\delta)$.

The width of the umbra δ_u is estimated as

$$\delta_u = \delta - z/(L/D) \qquad (7)$$

where z is the distance between the grid and the converter. The value δ = 3 mm was employed. When the object size is less than 150mm, the umbra width is 1 mm for *L/D* = 150, the value of the neutron radiography system in JRR-3M. Quantitative void fraction distribution can be measured by Eq.(4) after calculating the compensated attenuation terms in Eqs.(1)-(3) by Eq.(6) though the spatial resolution in y direction is reduce to 3 mm and the image information decreases to less than 1/3.

Measurement of the thickness of a step was carried out to show the efficiency of the present method. Fig.1 shows the grid and the step tested for the present report. The bars of the grid were made from B_4C fine powder less than 5 μm filled in thirty rectangular ducts 3 mm x 3 mm machined in an aluminum plate 5 mm in thickness. The step was made of acrylic resin and its thickness was varied from 2mm to 20 mm with 2mm interval. They are machined within 10 μm tolerance. The distance, z, between the converter and the step was varied from 0 to 90 mm by a remote- controlled traverser.

A cooled-CCD camera system at the JRR-3M in JAERI was used for the measurement. The exposure time was 6 seconds. The mathematical morphological filter was used to reduce star-like noises due to the direct irradiation of radioactive rays to the CCD elements. The measurement of the step thickness with and without the grid was carried out by changing the distance *z* from 0 to 90 mm.

The brightness of the step images,

$$S_s(x,y) = G(x,y)\exp\{-\rho_s\mu_{ms}t_s(x,y)\} + O_s(x,y) \qquad (8)$$

and the brightness without the step

$$S(x,y) = G(x,y) + O(x,y) \quad (9)$$

were measured.

The original visualized, filtered and quantitatively compensated images and the brightness distributions of the step are shown in Fig.2. It can be seen that the star-like noise and the effects of the scattering are well removed.

The attenuation rate plotted against the acrylic resin thickness is shown in Fig.3. The linearity more than 2 order can be obtained by the present method.

3. ACCURACY AND UNCERTAINTY ANALYSIS

The effects of the neutron scattering mentioned above depend on scattered neutrons in the object around the measured point. Therefore, the general accuracy of neutron radiography measurement cannot be determined but the accuracy of each measurement should be estimated.

The uncertainty of measurement in mechanical engineering is defined by the twice of the standard deviation of the measured values in the same condition. Confidence of the measurement is 95 % when the uncertainty is considered as the measurement error. The measured void fractions at the same condition may scatter since the phenomena fluctuate temporally and spatially. The measurement errors mentioned above should be discussed comparing with the uncertainty.

An aluminum pipe 10 mm in inner diameter, 1mm in thickness and 1 m in length was used for the two-phase flow experiments in a tube The grid made of B_4C bars 3 mm in width and 6 mm in interval. The original CCD camera image has many star-like noises due to the direct irradiation to the CCD chip and is brighter near the center due to the effects of neutron scattering. It was already shown that the star-like noises were well reduced to small noises by mathematical morphology filter and the brightness distributions are well compensated by the quantitative methods.

Ten images were taken for the same two-phase flow conditions at the exposure time of 4 seconds to calculate the standard deviation to discuss the uncertainty of the void fraction measurement. Uncertainty and comparisons with the standard correlations by drift flux model on void fraction measurement in the tube were discussed.

Fig.4 shows the measurement results of the water thickness in a tube used for two-phase flow experiment by the dots. The pixel size of the image was 0.1 mm. The solid line indicates the calculated thickness and the broken lines show $\pm$ 5% error lines. It can be seen that the water thickness distribution was measured within 5% errors except for near the wall where blur due to L/D of the neutron beam

caused the measurement error.

Fig.5 shows examples of cross-sectionally-averaged void fraction distributions of a slug flow in the tube. The measurement was carried for ten times at the same two-phase flow conditions to discuss the uncertainty. The void fraction fluctuates much in the slug flow. The uncertainties, which are defined twice of the standard deviations divided by the average value, of the void fraction distributions of the slug and the other flows are shown in Fig.6. They are around 20% for the slug flow while a few % for the other flows.

Experimental results on the void fraction were compared with the correlations by drift flux model. They are empirical equations fitted with the experimental data which often scattering by about 20 %. The results are shown in Fig.7 for each flow. The experimental results scatter 20 % for slug flows, 6 % for churn flows and 3 % for annular flows around the predicted values by the drift flux model. The same analyses were applied to the void fraction measurement in two-phase flow in the rod bundle as shown below. The cross-sectionally averaged void fraction distributions around the spacer was measured by ten times. The maximum uncertainty for the slug flow is about 10% and less than several % for the other flows.

Comparisons between the experimental results and the correlations by the drift flux model are shown in Fig.7. The measured values scatter 20 % for slug flows, 6 % for churn flows and 3 % for annular flows around the predicted values by the drift flux model.Both the uncertainties of the void fraction were less than several % for the churn and the annular flows and about 20 % for the slug flow. It was shown that the present quantitative measurement had enough accuracy since the practical empirical equations for the void fraction in two-phase flow were made with data scattered about 20 %.

The uncertainty was analyzed for the void fraction measurement in two-phase by neutron radiography. The measured data were compared with the correlations by the drift flux model. It is concluded that the accuracy of the void fraction measurement by neutron radiography is enough for two-phase flow researches especially for annular and churn flows in the present experiment. The accuracy depends on the two-phase flow conditions as well as the neutron radiography system. These analyses should be applied for each measurement in the other two-phase flow researches.

4. APPLICATIONS TO TWO-PHASE FLOW RESEARCHES

Quantitative void fraction measurement methods were applied to various two-phase flows and examples of the visualized images and the measurement results are shown as below:

(1) Two-phase flow in a tube and a concentric annular [10]

Radial void fraction distributions in a tube 10mm in inner diameter and concentric annular 10mm in outer diameter and 20 mm in inner diameter were measured by Abel transformation and CT

reconstruction and film layer thickness of the annular flows were determined as shown in Figs.8 and 9.

(2) Two-phase flow in a rod bundle [11]

A rod bundle with 4x4 simulating fuel rods 10 mm in outer diameter with circular ferule type spacers was visualized in Fig.10. Cross-sectionally averaged void fraction distributions were measured as shown in Fig.11. Fig. 12 shows that the void fraction measured in the developed regions agrees well with the drift flux model of a tube with an equivalent diameter. Examples of three dimensional void fraction distributions by CT reconstruction around the spacer were also shown in Fig.13.

(3) Two-phase flow in a plate heat exchanger [12]

Two-phase flows a stainless steel plate heat exchanger commercially sold were visualized and the void fraction distributions were measured as shown in Fig.14.

(4) Two-phase flow in a spiral tube [13]

Cross-sectionally averaged void fraction distributions and the centers of balance in cross section were measured as shown in Fig.15 to discuss the effects of the centrifugal force on the radial void fraction distribution in Fig.16.

(5) Two-phase flow in a tube with a spiral wire [14]

Cross sectional void fraction distributions in a tube 16 mm in inner diameter with a wire coil were measure by CT reconstruction to discuss the effect of two-phase flow on the heat transfer augmentation in Fig.17.

(6) Boiling two-phase flow in a capillary tube [15]

Freon was flushed in a capillary tube 2mm in inner diameter. Void fraction distributions were measured and pressure undershoot phenomena were discussed as shown in Fig.18.

5. CONCLUSION

A quantitative measurement method based on the umbra method was applied to the void fraction measurement of various two-phase flows. These results will be used to make new models and new correlations on the void fraction of two-phase flow.

References

1. Glickstein et al., Trans. ANS/ENS Vol.66, 1992, pp.591-593.
2. Hirdlika & Peterka, in "Neutron Radiography (3)", Kluwer Acad. Pub., 1990, pp.131-143.
3. Hibiki et al. J. Nucl. Sci. Tech. 30, 1993, pp.15-22.
4. Yoshii & Kobayashi Nucl. Instr & Meth. A377, 1996, pp.76-79.
5. Tamaki et al., in "Neutron Radiography (4)", Gordon & Breach Sci. Pub., 1992, pp.837-844.
6. Kobayashi et al. Proc. 1st. JSME/ASME Int. Conf. on Nuclear Engineering Vol.1, 1991, pp.649-654.
7. Murata et al., in "Neutron Radiography (4)", Gordon & Breach Sci. Pub., 1992, pp.583-590.
8. Takenaka et al., Nondestr. Test. Eval. Vol.16, 2001, pp.345-354.
9. Takenaka et al., Proc. 1st. European-Japanese Two-phase Flow Meet., 1997.
10. Takenaka et al., in "Neutron Radiography (7), Gordon & Breach Sci. Pub., to be published.
11. Takenaka et al., Nondestr. Test. Eval. Vol.16, 2001, pp.355-362.
12. Asano et al., Proc. German-Japanese Workshop on Multi-phase Flow, GJWMF 2002, Karlsruhe, Germany, Aug 27, 2002.
13. Asano et al., Nondestr. Test. Eval. Vol.16, 2001, pp.363-375.
14. Asano et al., in "Neutron Radiography (7), Gordon & Breach Sci. Pub., to be published.
15. Asano et al. Nucle. Instr. & Meth., A424, 1999, pp.98-103.

Nomenclatures

G(x,y) : gain distribution of image
j : volumetric flux [m/s]
J : total volumetric flux [m/s]
L/D : rate of length between neutron source and converter to size of neutron source, proportional to neutron beam parallelness
O(x,y) : offset distribution of image
S(x,y) : image brightness distribution
t(x,y) : thickness distribution [m]
u : velocity [m]
(x,y) : coordinates in image
z : distance in neutron beam direction [m]

Greek
α : void fraction
δ : width and interval of bars in a grid [m]
μ_m : mass attenuation coefficient [m^2/kg]
ρ : density [kg/m^3]
σ : standard deviation

suffixes

0 : filled with liquid, α =1
1 : filled with gas, α =0
c : compensated
g, G : gas
l, L : liquid
TP : two-phase
u : umbra
w : wall

List of Figure Captions

$$\delta_L = "Center\ of\ liquid\ mass" = \sum_{i=1}^{n}\left[(t_L)_i r_i\right] \Big/ \sum_{i=1}^{n}(t_L)_i$$

$$F_G = \overline{\alpha}\rho_G g\cos\theta + \overline{\alpha}\rho_G {u_G}^2 / R$$

$$F_L = (1-\overline{\alpha})\rho_L g\cos\theta + (1-\overline{\alpha})\rho_L {u_L}^2 / R$$

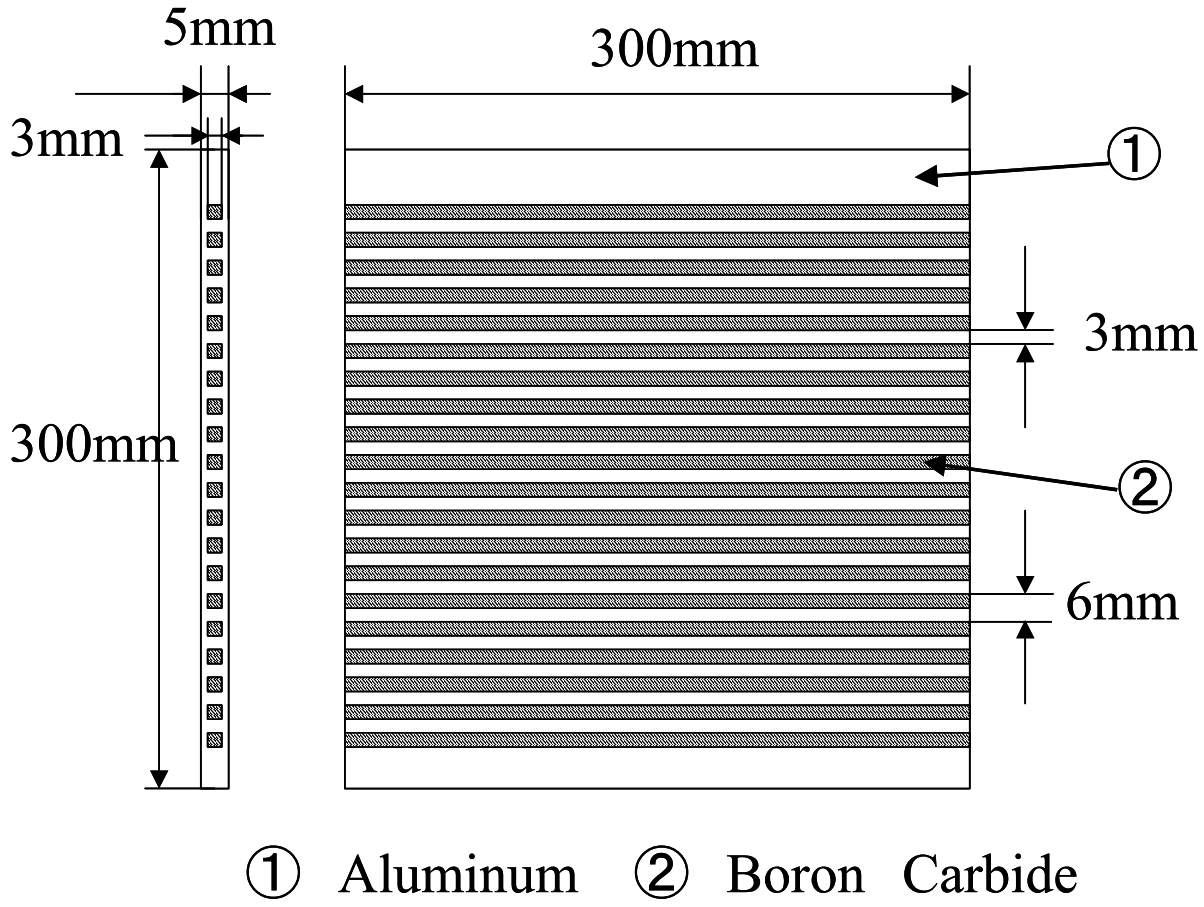

Fig.1 Grid made of boron carbide, δ =3mm

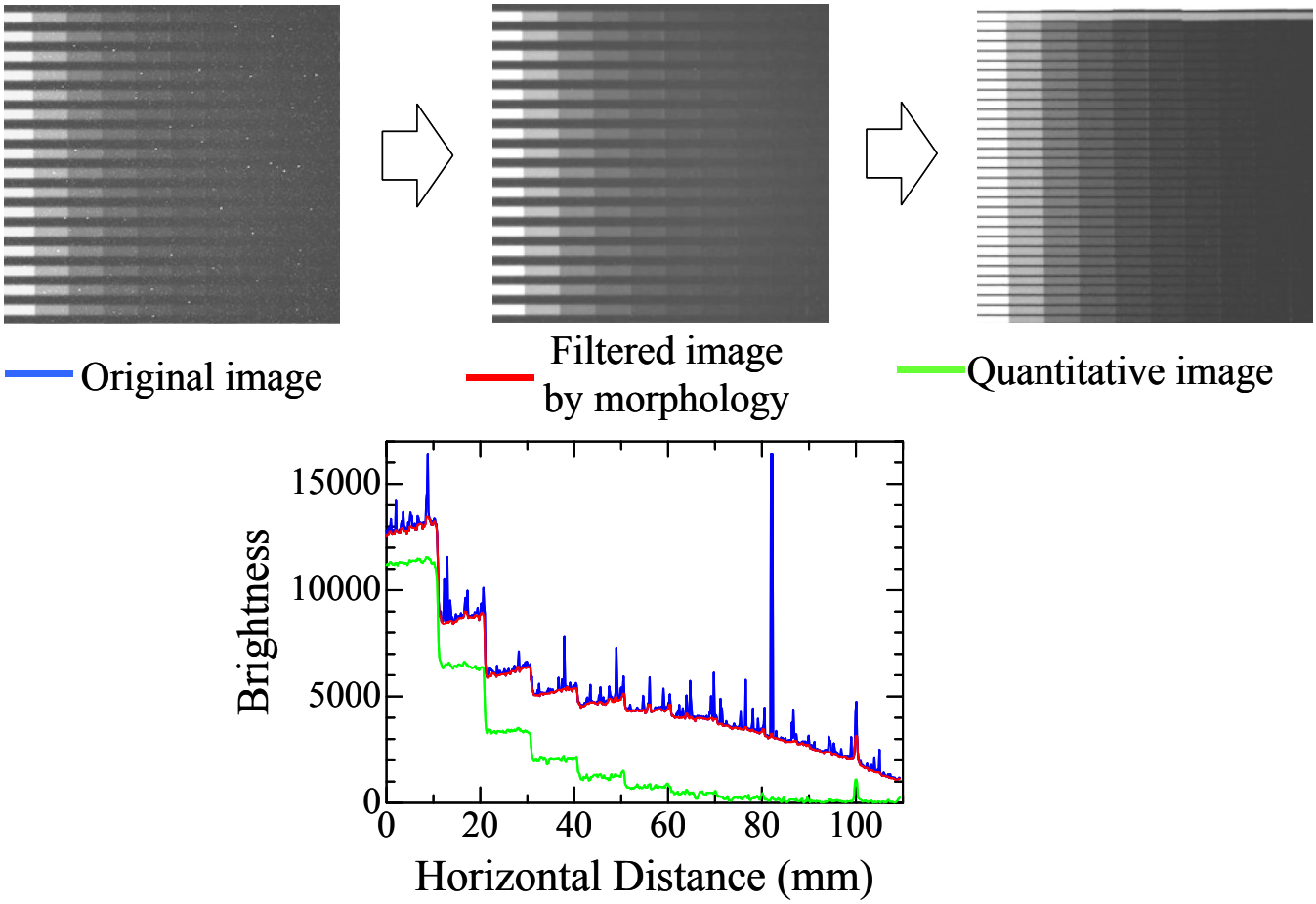

Fig.2 Processed images and brightness distribution

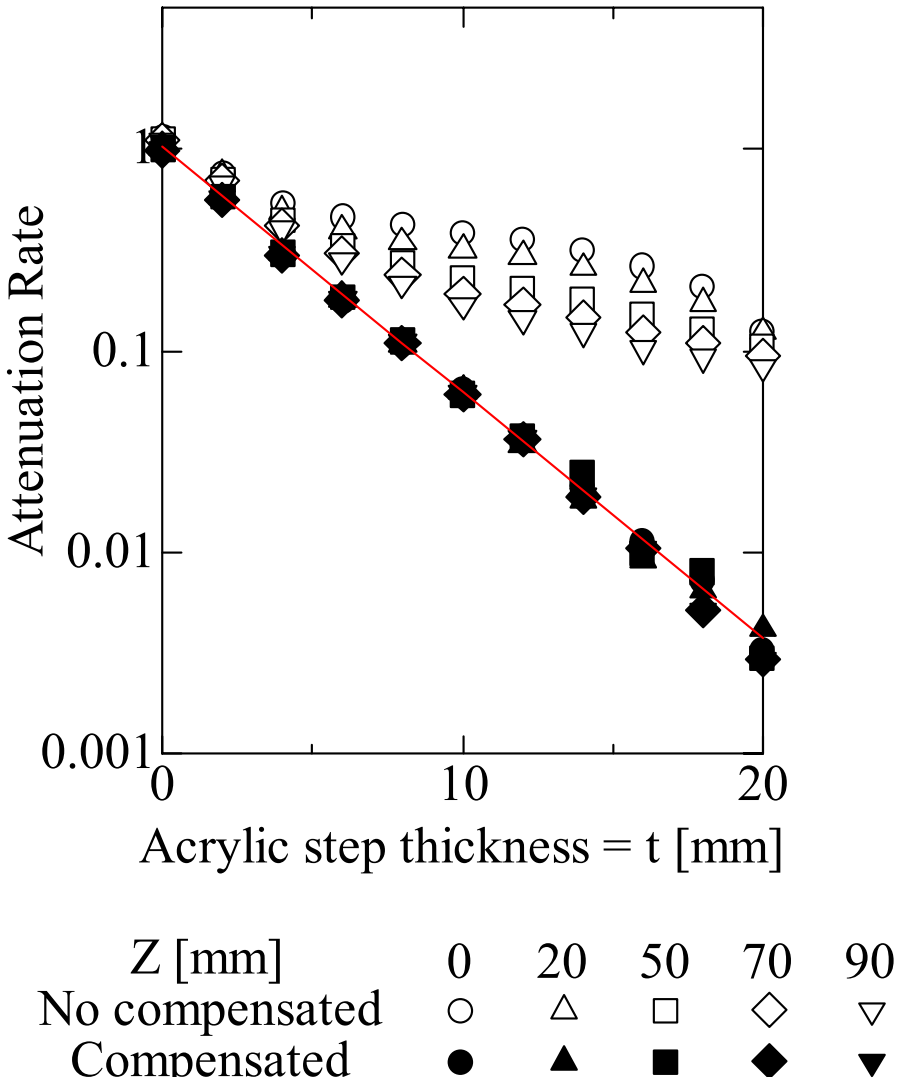

Fig.3 Attenuation rate in acrylic resin step

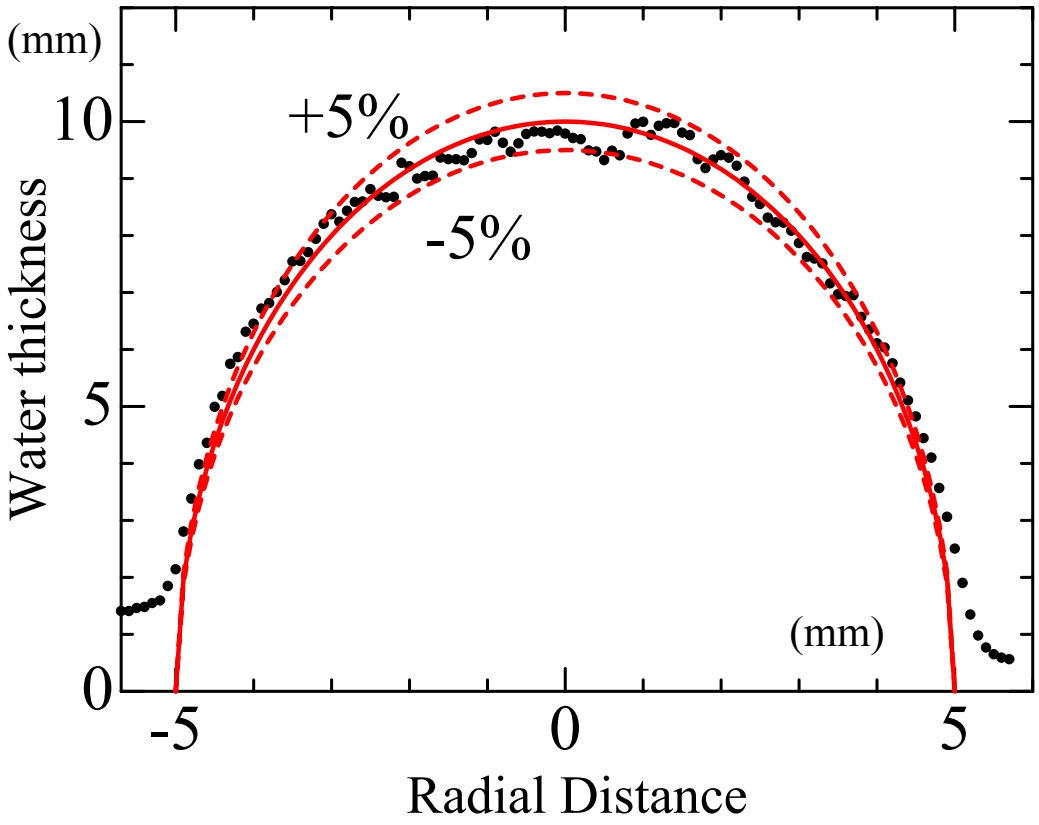

Fig.4 Measurement of water thickness in a tube

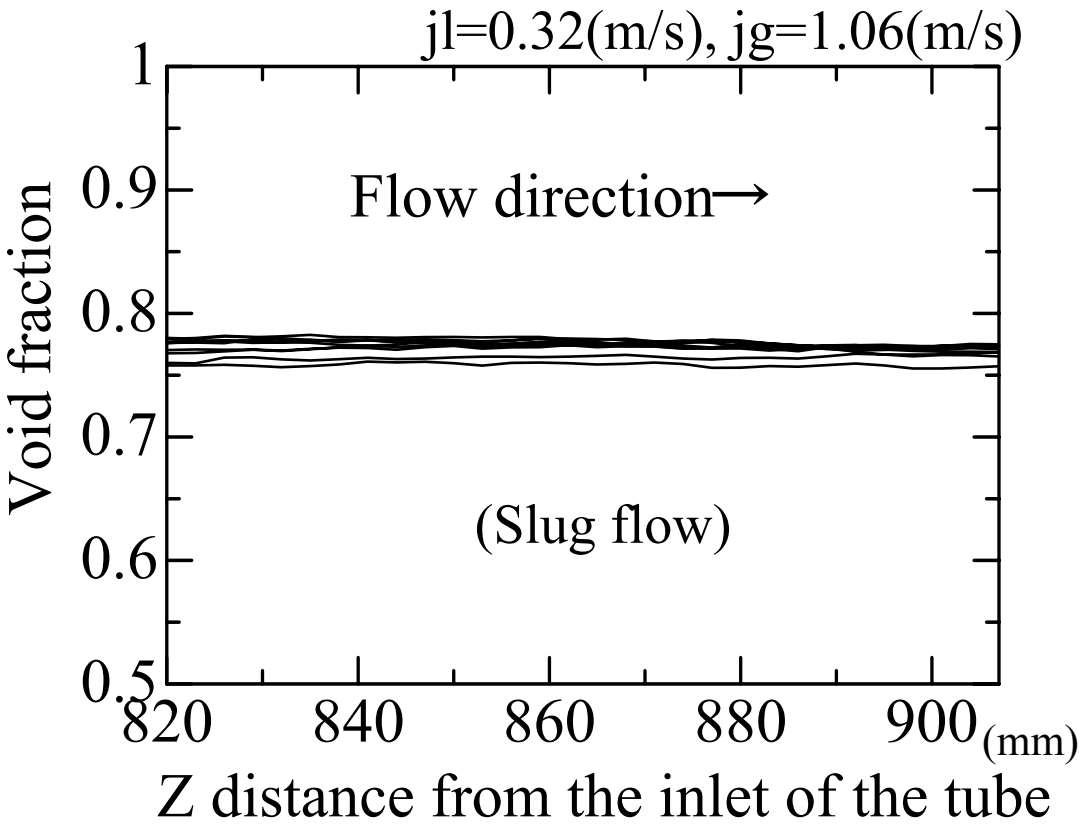

Fig.5 Cross sectionally averaged void fraction distribution measure for ten times for the same condition

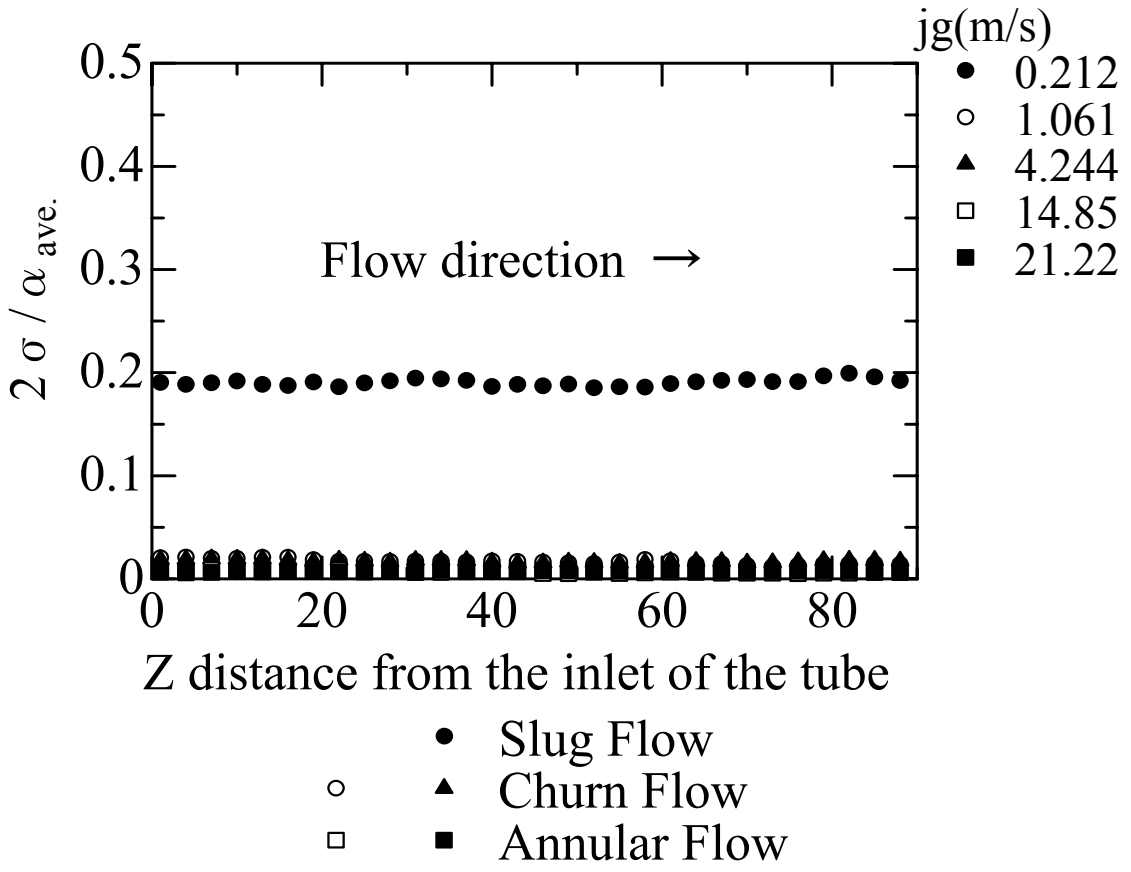

Fig.6 Uncertainty rate

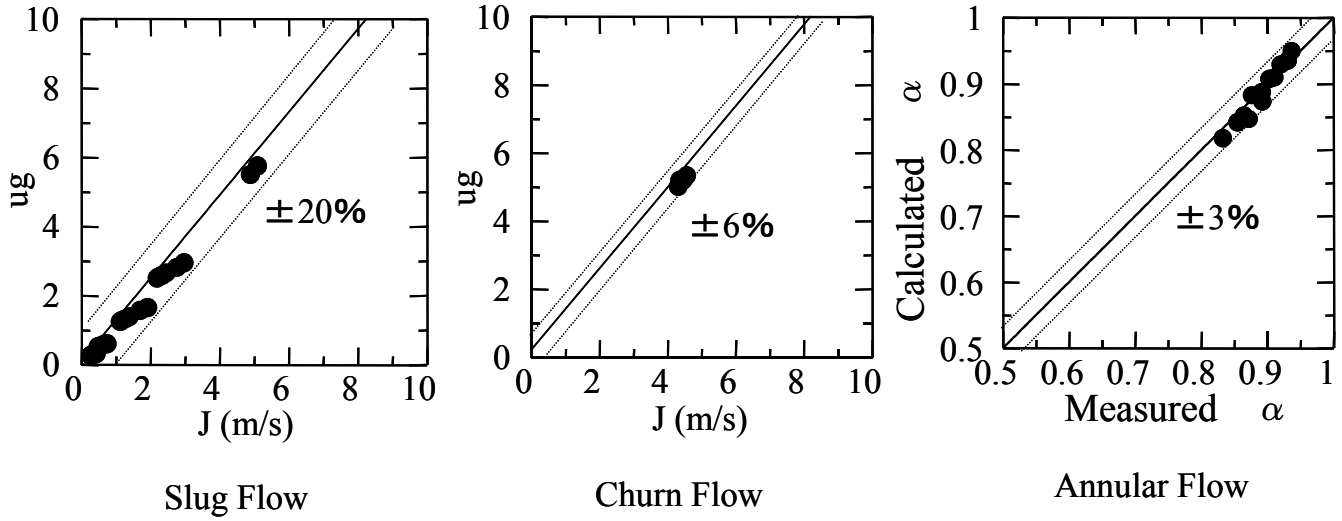

Fig.7 Comparison of measured void fraction to drift flux model

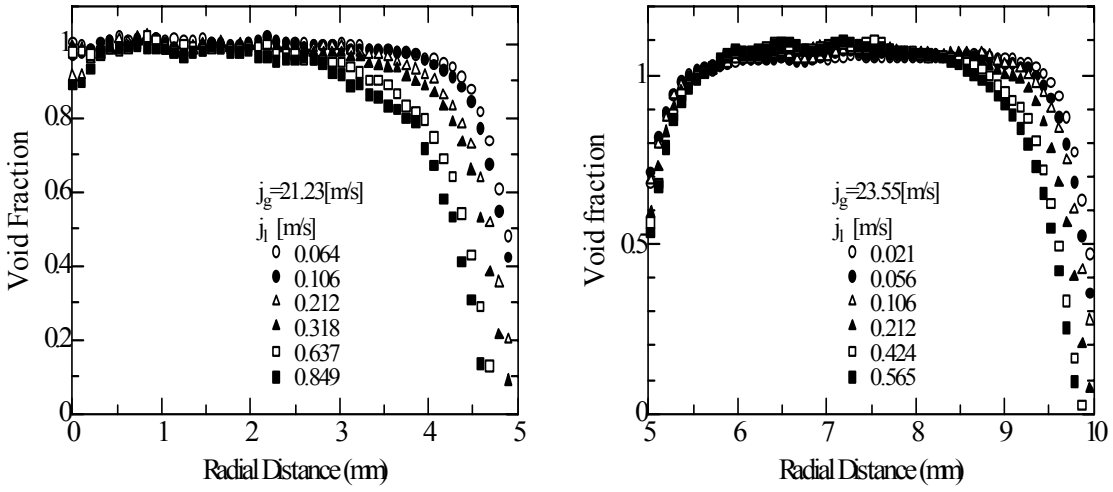

(a) tube (b) concentric annular

Fig. 8 Radial distributions of void fraction in a tube and a concentric annular (1)

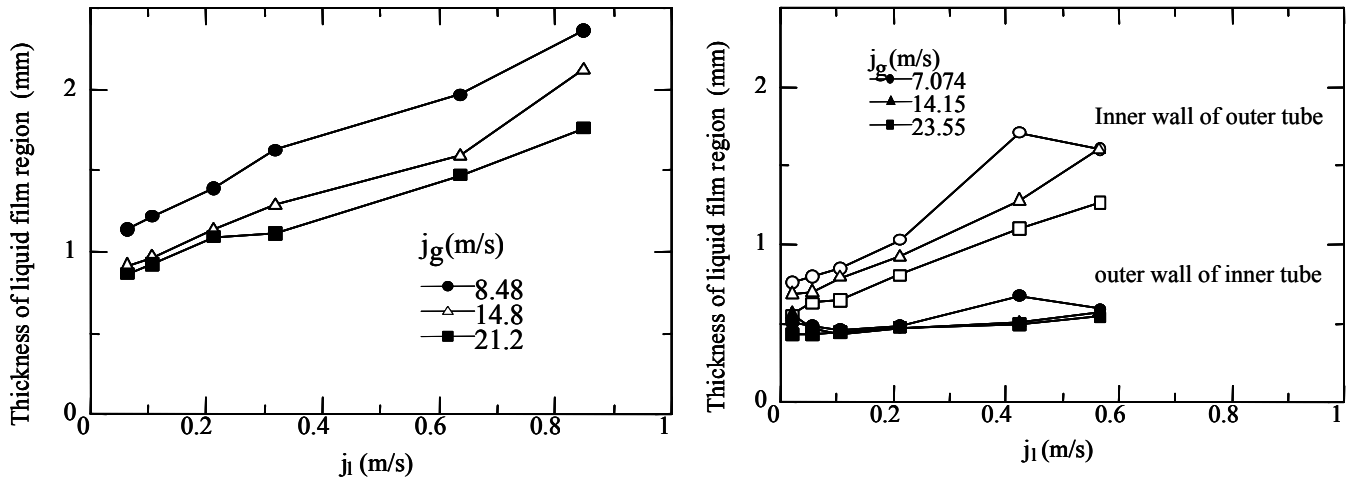

(a) tube (b) concentric annular

Fig. 9 Thickness of liquid film region of annular flow in a tube and a concentric annular (1)

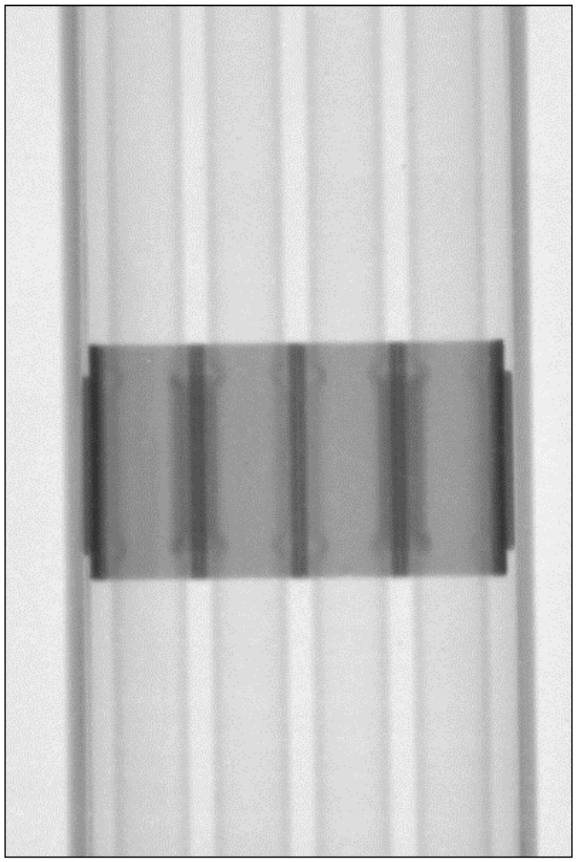

(a) without two-phase flow

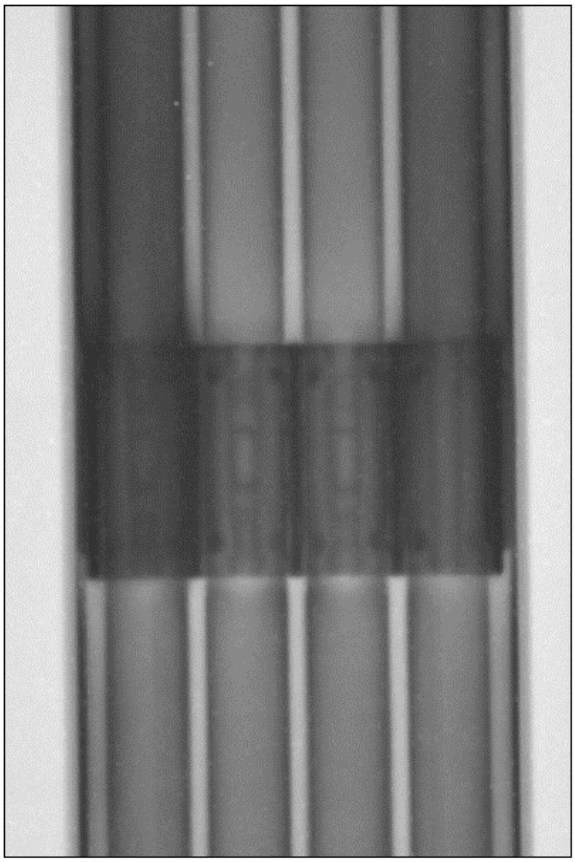

(b) with two-phase flow

Fig.10 Visualization of 4x4 rod bundle (2)

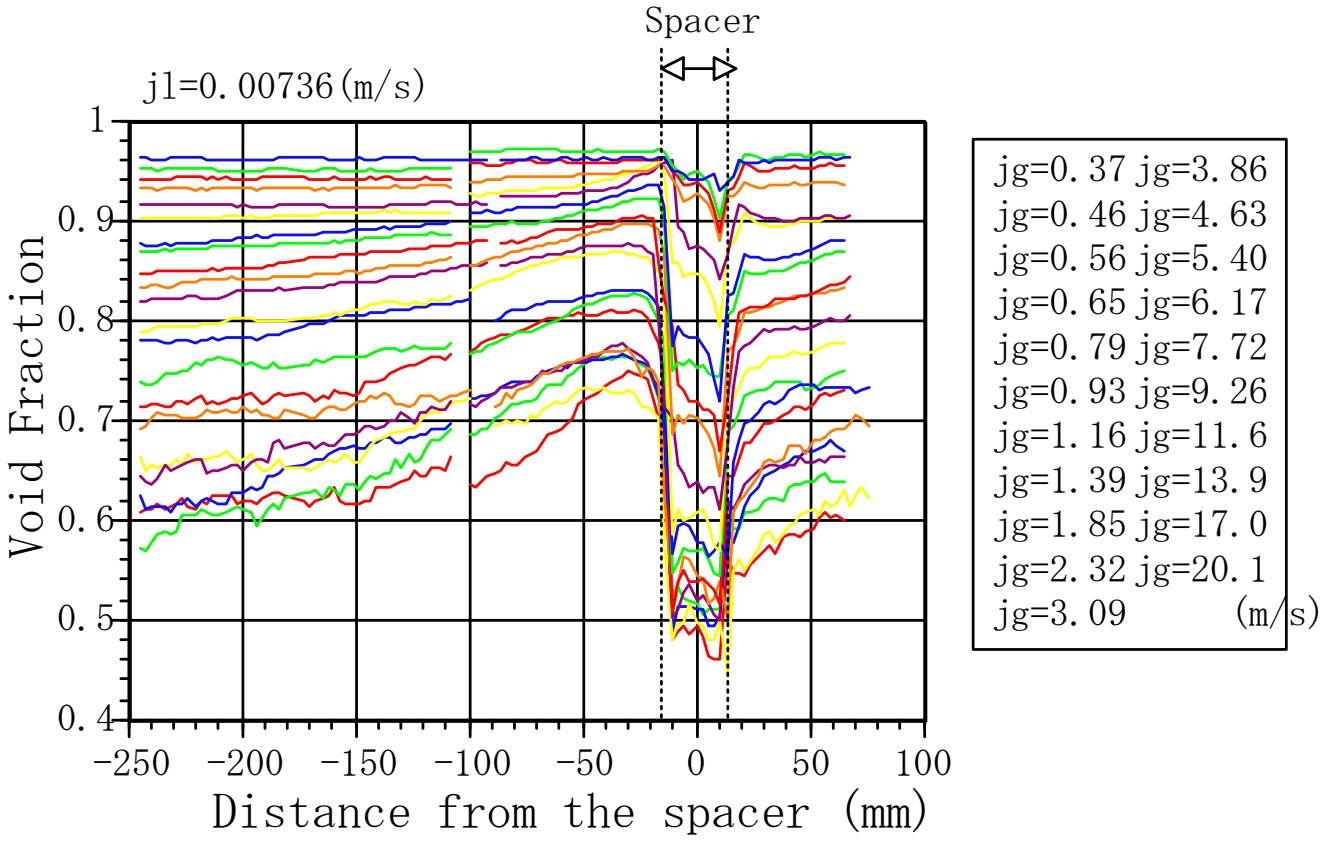

Fig.11 Cross sectionally averaged void fraction distributions near the spacer (2)

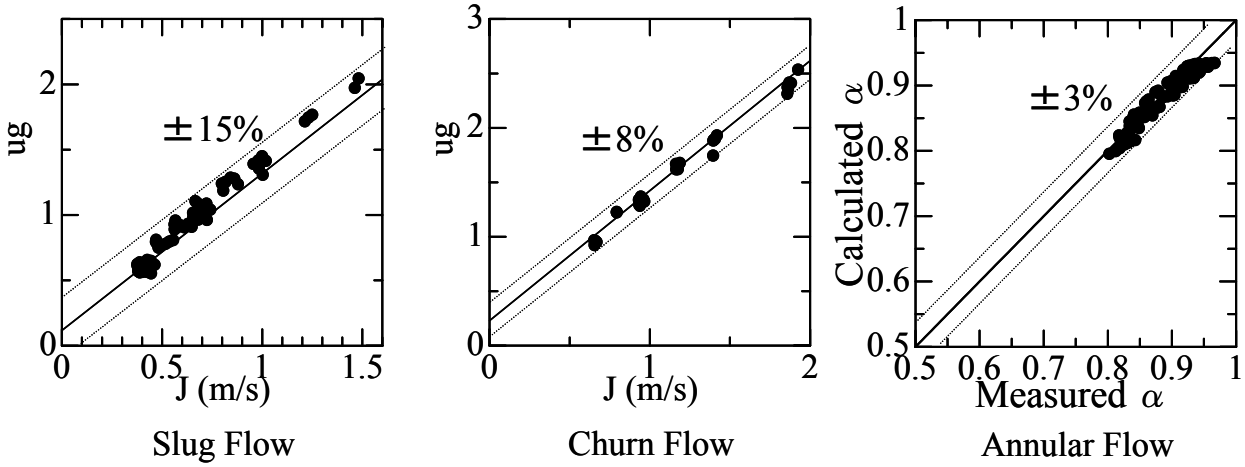

Fig. 12 Comparison with drift flux models in the developed region (2)

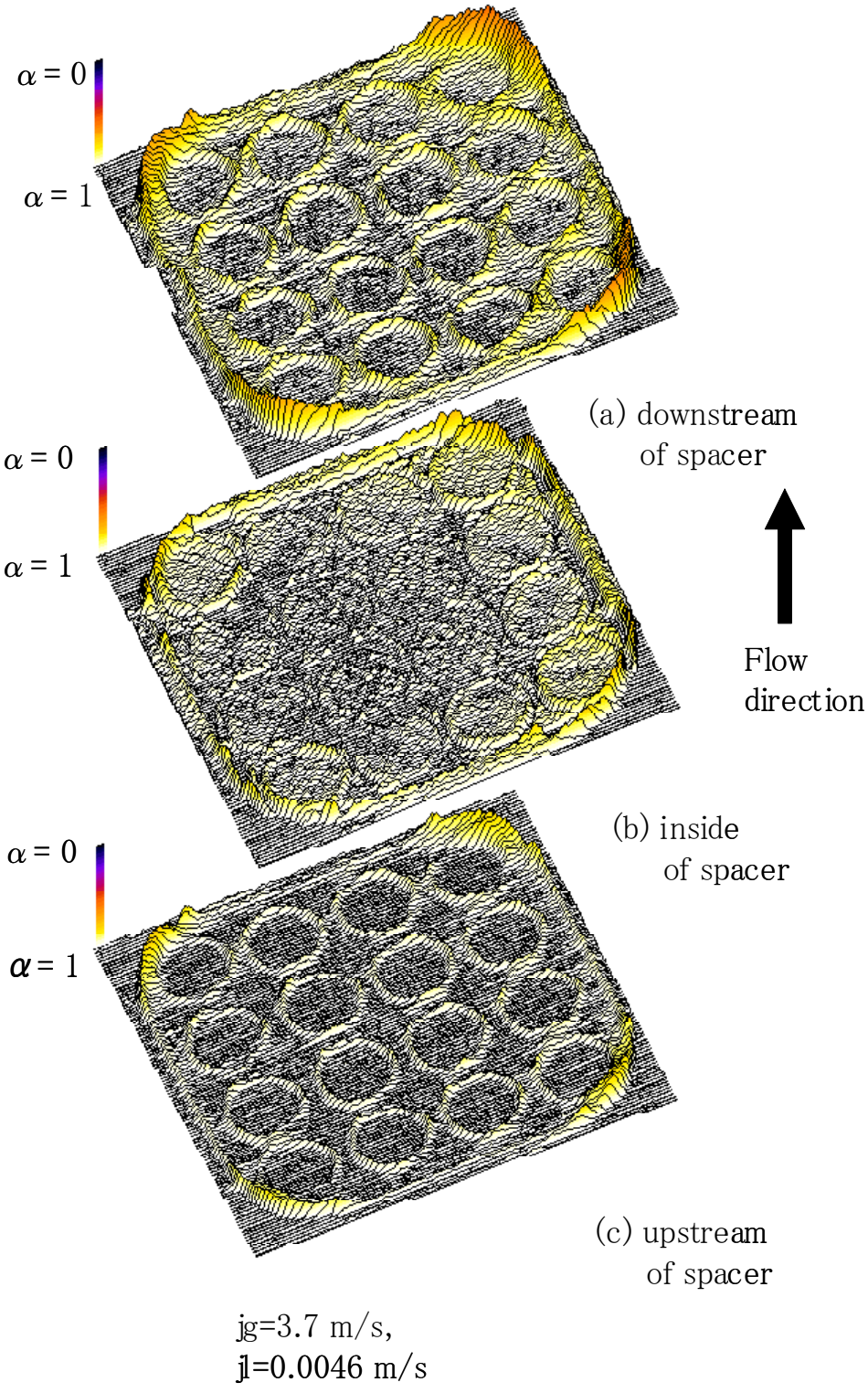

Fig.13 3-D void fraction distribution (2)

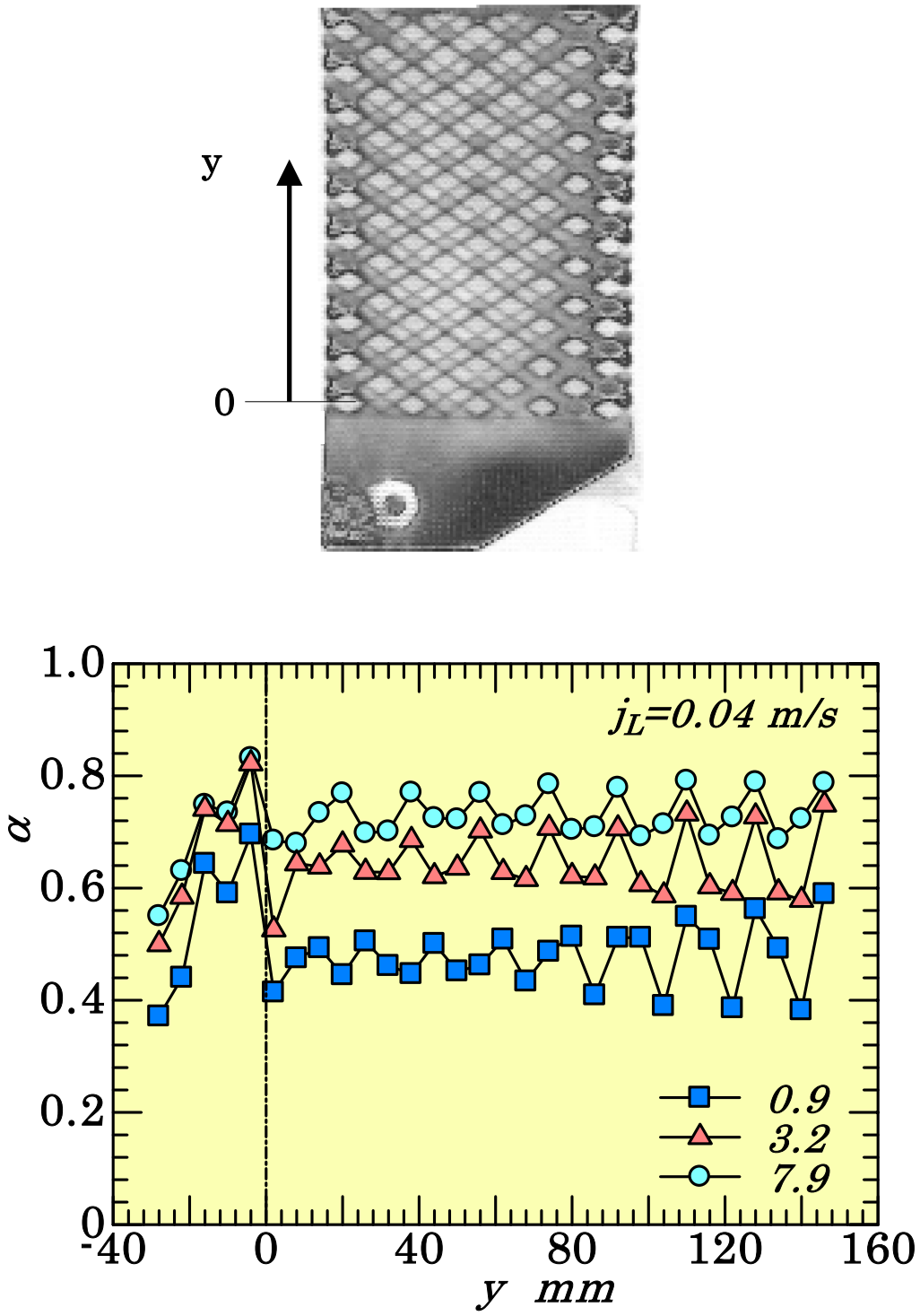

Fig.14 Void fraction distributions in a plate heat exchanger (3)

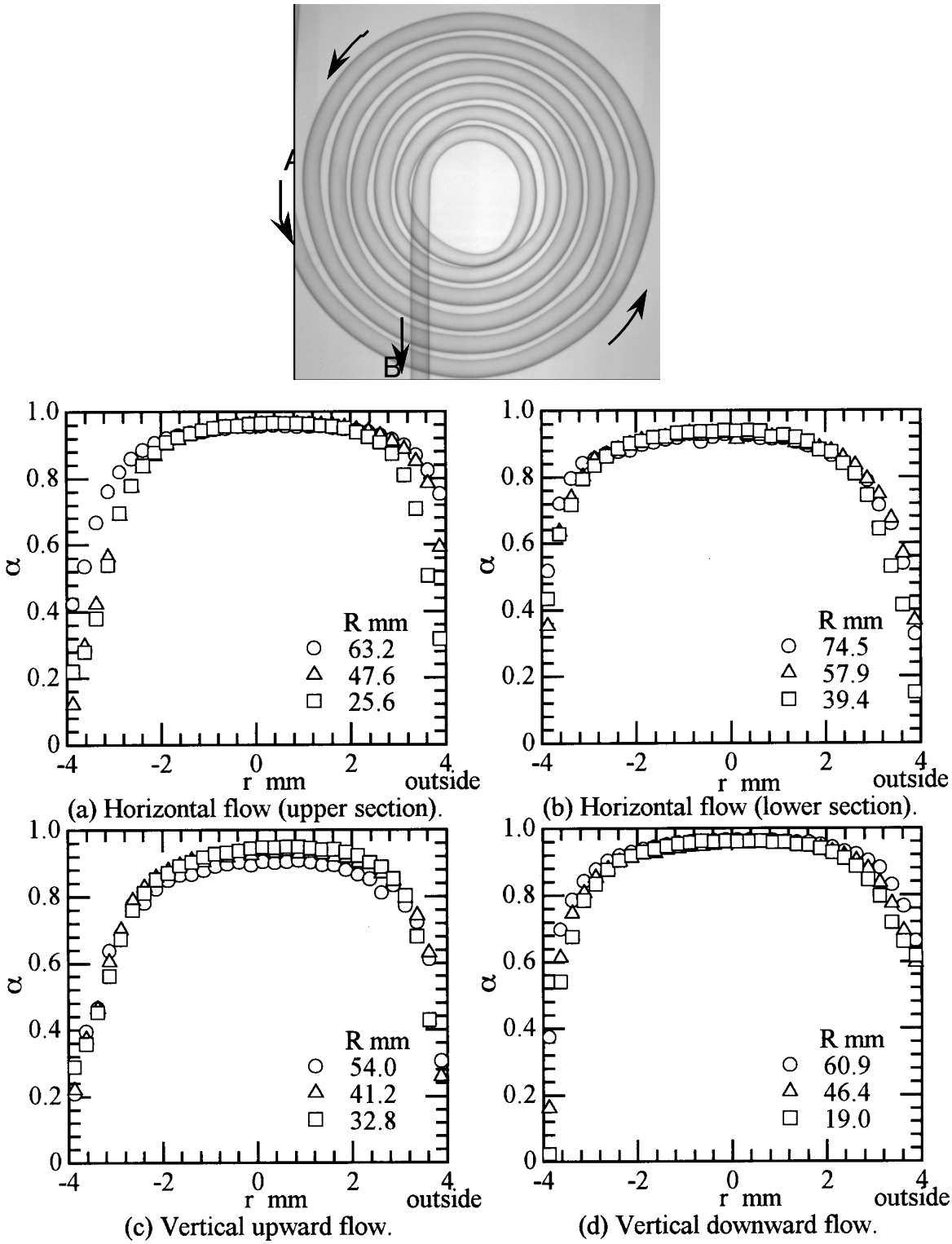

Fig.15 Void fraction distributions in a spiral tube (4)

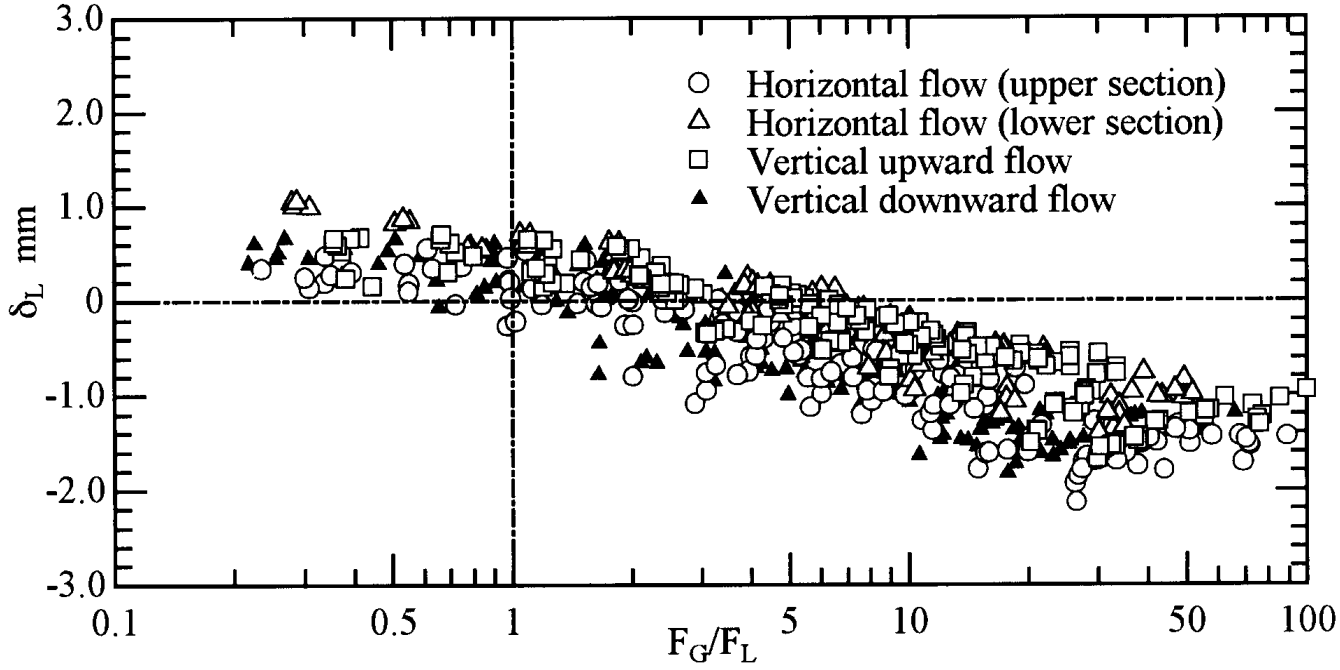

$$\delta_L = \text{"Center of liquid mass"} = \sum_{i=1}^{n}\left[(t_L)_i r_i\right] \Big/ \sum_{i=1}^{n}(t_L)_i$$

$$F_G = \overline{\alpha}\rho_G g\cos\theta + \overline{\alpha}\rho_G {u_G}^2 / R$$

$$F_L = (1-\overline{\alpha})\rho_L g\cos\theta + (1-\overline{\alpha})\rho_L {u_L}^2 / R$$

Fig.16 Center of liquid mass in the cross section of the spiral tube (4)

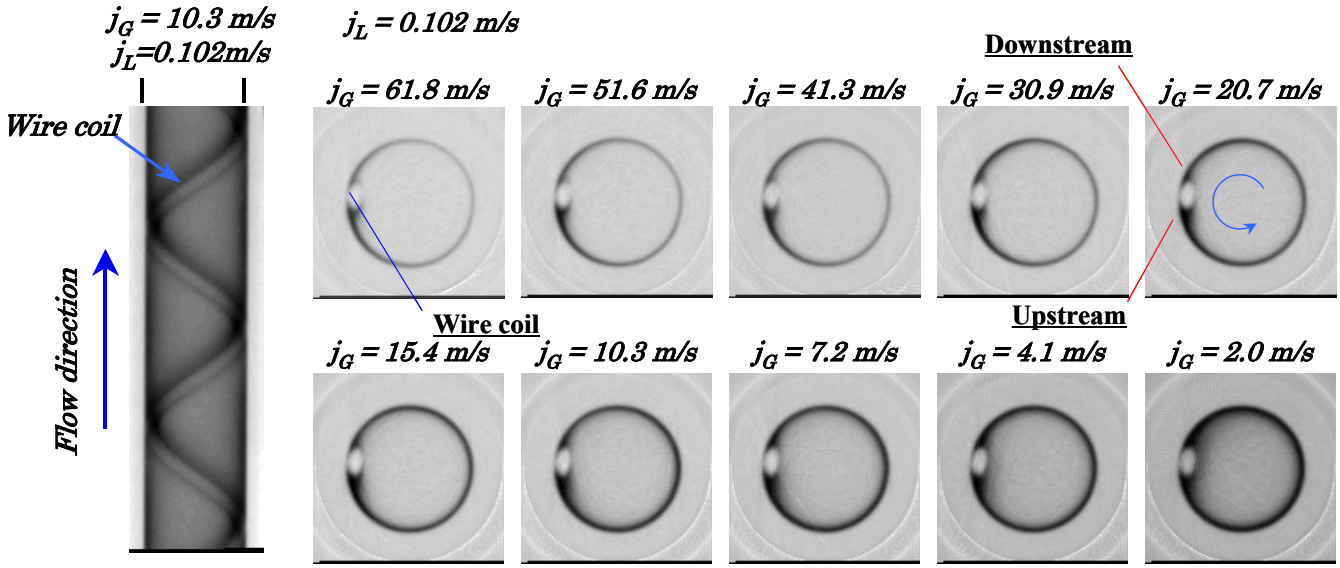

Fig.17 Void fraction distributions in a tube with a spiral wire (5)

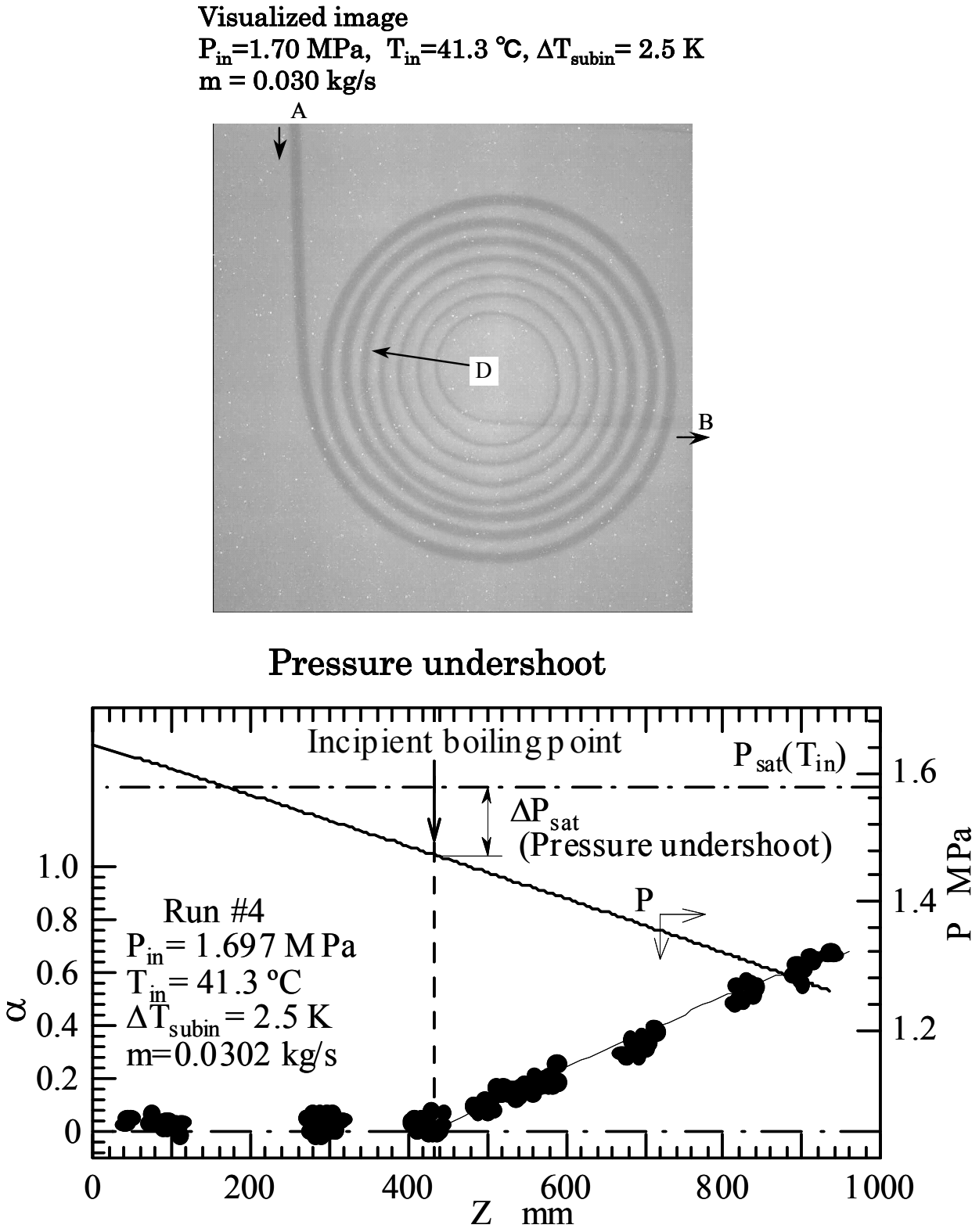

Fig. 18 Void fraction distributions of Freon flushing flow in a spiral capillary tube and estimation of pressure undershoot (6)